The impact of horizontal resolution on the tropical heat budget in an Atlantic ocean model

Markus Jochum,
(Massachusetts Institute of Technology)
Raghu Murtugudde,
(Earth System Science Interdisciplinary Center)
Raffaele Ferrari,
(Massachusetts Institute of Technology)
Paola Malanotte-Rizzoli
(Massachusetts Institute of Technology)

8/5/04
accepted in Journal of Climate

Corresponding author's address:
markus@ocean.mit.edu, 617-2533573
MIT, 77 Massachusetts Avenue, 54-1410,
Cambridge, 02138 MA

Abstract: An ocean general circulation model (OGCM) of the tropical Atlantic is coupled to an advective atmospheric boundary layer model. This configuration is then used to investigate the hypothesis that resolving tropical instability waves (TIWs) in OGCMs will remove the equatorial cold bias that is a feature common to coarse resolution OGCMs. It is shown that constant horizontal diffusivity in coarse resolution models is a reasonable approximation to the equatorward heat transport by tropical instability waves. However, this diffusion leads to a warmpool that is too cool by approximately 1K. It is demonstrated that the reason for this is that diffusion removes heat from the warmpool to heat the equatorial cold tongue, whereas TIWs draw their heat mostly from the atmosphere, not from the warmpool as hitherto assumed, and thus can bring more heat to the equatorial cold tongue without cooling the warmpool. The equatorial warming due to TIWs is slightly larger than the warming due to diffusion but this increased equatorial heat flux in the high resolution experiment is compensated by increased equatorial entrainment there. This is attributed to the Equatorial Undercurrent being stronger, thereby increasing the entrainment rate through shear instability. Thus, higher resolution does not significantly increase the total oceanic heat flux convergence in the equatorial mixed layer. The different resolution does, however, lead to changes in the atmospheric heat flux convergence, because the sharper cross-equatorial temperature gradient in the high resolution experiment leads to reduced latent and sensible heat losses over the equator.

1 Introduction

SST is the principal ocean variable that affects the atmosphere. Prediction of the coupled ocean-atmosphere variability will always be limited by our ability to predict SST. To date, a rather impressive operational prediction of interannual variability of the coupled system has been achieved (Cane et al., 1986). However, shortcomings still remain (Davey et al., 2002). Especially in the tropics the strong ocean-atmosphere feedback processes make it difficult to decide which model component is most in need of improvement: the ocean model, the atmosphere model or the representation of air-sea interaction. The situation is further complicated by the large uncertainty of observed heat fluxes (Blumenthal and Cane, 1989).

To understand the shortcomings of an ocean general circulation model (OGCM) in simulating SST one would ideally analyze an OGCM not coupled to an atmospheric general circulation model. However, it is common practice in uncoupled models to use boundary conditions that restore SST to climatological values or to use bulk parameterizations with specified air temperature and humidity; both choices mask potential errors in the oceanic mixed layer heat budget. However, coupling the OGCM to an atmospheric boundary layer model (ABLM) such as that of Seager at al. (1995) removes these problems. Provided with observed wind velocity, SST and incoming solar radiation the ABLM determines the atmospheric advection of heat and moisture and thereby the air-sea heat fluxes. Thus, the OGCM has much more freedom to develop its own SST and the SST reflects ocean physics rather than the constraints imposed by the boundary conditions.

Murtugudde et al. (1996) coupled this ABLM to the Gent and Cane (1989) OGCM and demonstrated that advection and diffusion of moisture play a significant role in determining the tropical SST in all three oceans. More importantly, at least in the context of the present study, the ABLM enabled them to determine that the main model flaw is the inadequate representation of the equatorial cold tongue (ECT) in the Atlantic and Pacific. Stockdale et al. (1993), too, suggested that a too cold ECT is a critical factor in compromising the skill of OGCMs used in climate studies. Similarily, Davey et al. (2002) showed that the misrepresentation of the SST in the ECT is a general deficiency of OGCMs coupled to atmospheric models.

Since Hansen and Paul (1984) it is known that equatorial mesoscale eddies (commonly referred to as tropical instability waves, TIWs) can make a significant contribution to the equatorial mixed layer heat budget. Based on the results of these observations and the coarse resolution OGCM studies, we arrive at the following hypothesis: Resolving the TIWs in OGCMs will remove the cold bias of the ECT. For the present study it is assumed that the eddy resolving OGCM realistically reproduces equatorial ocean dynamics and that shortcomings of the non-eddy resolving OGCM are due to an inadequate parameterization of subgrid

scale processes. It is focused on the Atlantic ocean, but since the phenomena dominating the heat budget (trade winds, ECT and TIWs) are similar in the Pacific ocean, the results of this study should apply there as well, at least qualitatively. For a recent discussion of the observed heat fluxes in the tropical Atlantic, see Foltz et al. (2003); however the sharp equatorial gradients and high temporal variability in the ECT can only be resolved with an OGCM.

The next section will describe the OGCM and the experiments, the third section discusses the equatorial heat budget in the different experiments and the last section summarizes the results and their implications.

2 Model description

The OGCM employed for this study is the reduced gravity, primitive equation model of Gent and Cane (1989), which was specifically designed for studying the interactions between the dynamics and the thermodynamics of the upper tropical oceans. This model introduced an approach to efficiently achieve fine vertical resolution below the mixed layer in regions of high vertical shear. The vertical structure of the model consists of a mixed layer above a fixed number of sigma layers.

The mixed layer depth and the thickness of the last sigma layer are computed prognostically and the remaining layers are computed diagnostically such that the ratio of each sigma layer to the total depth below the mixed layer is held to its prescribed value. The Lorenz N-cycle scheme (Lorenz, 1971) is used for time-integration and a 8th order scale-selective Shapiro Filter provides horizontal friction and diffusion. The lowest order Shapiro Filter is equivalent to Laplacian diffusion, higher orders are more scale selective (Gent and Cane, 1989) but have the drawback that the contribution of diffusion to the heat budget cannot be easily recovered from the model results. To optimize the model solution, a high order filter was chosen nevertheless, and the diffusion of heat was estimated as the residual of the heat budget. The danger of this approach is that errors in the calculation could be misinterpreted as diffusion; however, the next section will show that the resulting diffusion in the high resolution experiment is so small that we can be confident of our results.

A hybrid vertical mixing scheme was developed and embedded in the model by Chen et al. (1994). The traditional bulk mixed layer model of the Kraus-Turner (1967) type is combined with the dynamic instability model of Price et al. (1986) to simulate the three major processes of oceanic turbulent mixing: The bulk mixed layer model relates the atmospheric forcing to the mixed layer entrainment/detrainment; the gradient Richardson number mixing accounts for the shear flow instability; and an instantaneous adjustment simulates convection in the ther-

mocline.

The OGCM is coupled to an ABLM that is described in Seager et al. (1995). Within this atmospheric mixed layer, the air temperature and air humidity are determined by a balance between surface fluxes, horizontal advection by prescribed winds, entrainment from above the mixed layer and radiative cooling. This approach to determine the surface heat fluxes represents a clear improvement to the more traditional restoring boundary condition without the computational expense of a complete coupled model (Murtugudde et al., 1996).

For the present study it must be emphasized that with the ABLM the OGCM has more liberty to seek its steady state than with traditional surface boundary conditions like SST restoring or prescribing the surface heat flux. Especially the advection of heat and moisture within the ABLM creates nonlocal effects in the heat budget. The ocean heat budget then becomes more complex but allows for a better understanding of the SST. This is because differences in the SST of different experiments are not artificially changed by the boundary conditions. One consequence of using the ABLM is that each experiment computes its own latent and sensible heat flux, potentially creating large changes in the heat budget of seemingly similar model setups.

In previous studies this model has demonstrated its ability to reproduce the observed SST and circulation in the tropical Atlantic (Murtugudde et al., 1996; Inui et al., 2002) as well as the variability of the eddy field (Jochum et al., 2004b). The model is initialized with Levitus (1994) temperature and salinity fields, driven by monthly mean climatological Hellerman and Rosenstein (1983) winds, and its salinity and temperature are restored to Levitus (1994) in northern and southern sponge layers at 25^oN and 25^oS, respectively. Solar radiative forcing is taken from the Earth Radiation Budget Experiment (Li and Leighton, 1993), the cloud data is taken from Rossow and Schiffer (1991) and the precipitation is based on Xie and Arkin (1998). The evaporation is determined by the ABLM. The model has 8 layers in the vertical for an average total depth of 600 m. The model is spun up for 20 years and the results discussed in the paper are taken from the subsequent 5 years of simulation. Two experiments are performed: a high resolution experiment (H) with $\frac{1}{4}$ degree horizontal resolution and a low resolution experiment (L) with 1 degree horizontal resolution. The model setups were identical otherwise. However, since the horizontal diffusion is determined by the Shapiro filter, which is of the same order in both runs, the effective horizontal diffusion is larger in L than in H because of the coarser resolution in L. This could be interpreted as representing the effect of the eddies in H that are not resolved in L, but this is not the whole story as will be discussed in the next section.

The annual mean SST and the variance of the meridional velocity on intra-annual timescales at the surface are shown for H in Figure 1. In L, there is negligible eddy activity and the annual mean SST is lower everywhere (up to 1.5 K, see

next section). While the low eddy activity is to be expected in L, the lower SST is surprising and is explained in the next section. As motivated in the introduction, the present study will focus on the equatorial mixed layer and conclusions are restricted to this area only. Outside the deep tropics the larger SST in H has probably different causes than the ones presented in the next section. For example, Nurser and Zhang (2000) and Oschlies (2002) discuss how in midlatitudes baroclinic instability can raise the SST.

3 The mixed layer heat budget

Jochum et al. (2004a, JMB hereafter) showed that the observed meridional eddy heat flux convergence due to the TIWs (e.g. Hansen and Paul, 1984) can partly be compensated by the associated vertical eddy heat flux. The equatorial ML, however, is so thin that even the residual eddy heat flux of approximately 30 W/m^2 (in their model) is an important component of the heat budget. The hypothesis underlying the present study is that resolving the equatorial mesoscale eddy field (mainly TIWs, see Weisberg and Weingartner, 1988; Foltz et al., 2004; JMB) will improve the representation of the ECT and remove the equatorial cold bias observed in coarse OGCM. Because of the complexity of the equatorial heat budget, simple physical reasoning might mislead any guesses of the impact of TIWs on the equatorial SST. A more satisfactory approach is to compare the TIW resolving experiment H with the non-eddy resolving experiment L.

The strip between 25^oW and 20^oW is best suited for the analysis because it crosses the ECT and the warmpool to its north without crossing land. These two areas are of central importance to the tropical Atlantic variability (Zebiak, 1993; Chiang et al., 2002) and representing their SST correctly is key to make progress in modeling tropical Atlantic variability. Increasing the resolution only marginally changes the mixed layer depth (Figure 2) but significantly increases the SST and the equatorward SST gradient (Figure 3). The comparison with the observations leads to the conclusion that the overall SST is improved but that the cold tongue is still too cold. Also, the SST difference between the warm pool and the cold tongue in H is larger than in the observations of any single year (not shown). Contrary to the expectations, increasing the resolution leads to an improvement of the SST in the warm pool and not in the cold tongue. The following analysis of the heat budget will explain this result and lead to a new understanding of the role of TIWs in the equatorial heat budget.

The heat budget for the mixed layer (ML) is:

$$c_p \rho h (T_t + \mathbf{v} \cdot \nabla \mathbf{T}) = Q_{atmos} - Q_{ent} + Q_{diff} \tag{1}$$

(after Stevenson and Niiler, 1983).

T is the SST, ρ is the density and c_p the heat capacity of seawater, h the ML depth, v the horizontal velocity vector, Q_{atmos} the net surface heat flux convergence from the atmosphere, Q_{ent} the cooling of the ML due to entrainment of water from below and Q_{diff} the horizontal diffusion of heat in the OGCM, intended to represent unresolved eddy transports. Dividing by $c_p \rho h$ and averaging over the 5 years of model output yields:

$$\overline{\mathbf{v_s} \cdot \nabla \mathbf{T_s}} + \overline{\mathbf{v_s} \cdot \nabla \mathbf{T'}} + \overline{\mathbf{v'} \cdot \nabla \mathbf{T_s}} + \overline{\mathbf{v'} \cdot \nabla \mathbf{T'}} = \overline{q_{atmos}} - \overline{q_{ent}} + \overline{q_{diff}}, \tag{2}$$

where the overbar denotes the 5 year mean; the SST and the velocities have been split into mean plus seasonal cycle (subscript s) and eddy component (superscript '). The seasonal cycle has been determined by averaging over the monthly values of all years, the eddy components are the deviations from these seasonal values. The first term on the *lhs* is the contribution of the mean and the seasonal cycle to the heat budget, the next three terms are the eddy contributions (since they would be zero without eddies, see Kessler et al., 1998). The reason for this somewhat unusual split is that it facilitates the comparison between L, which can be expected to reproduce the seasonal cycle but not the eddy fluxes, and H which resolves both. The components of the budget in (2) can be computed from the model output to estimate what processes determine the SST.

The heat budget for H (Figure 4) is similar to the one obtained by JMB who studied an eddy resolving level model (MOM2b) driven by the same winds as H but with SST restoring as thermal boundary condition and the Pacanowski and Philander (1981) vertical mixing scheme. The main difference is that the TIW contribution to the ML heat budget in JMB is 50% smaller than in H and the mean advection of heat in H is 50% smaller than in JMB. The contribution of entrainment and atmospheric net heat flux are approximately equal. Given the very different vertical mixing parameterization and thermal boundary conditions in the 2 experiments, this is a reassuring result. However, one of the motivations of the present study is that in JMB the ML is not properly resolved and the SST restoring introduces spurious heat sources. These shortcomings are overcome in H as described in the previous section.

The similarity of the mean and seasonal advection of heat (red line in Figures 4 and 5) in H and L demonstrates that the seasonal signal is well resolved in L and that the scale separation between the seasonal and high frequency signals is large enough to justify the split in Equation (2). North of the equator, the mean and seasonal heat advection is dominated by the meridional component that moves upwelled cold water polewards through Ekman dynamics, whereas south of the equator zonal and meridional advection are approximately of equal importance. On and near the equator (1^oS to 1^oN) zonal advection dominates, which is in accordance with the observations by Foltz et al. (2003).

Comparing Figures 4 and 5 shows that the lower SST in the warmpool of L

is caused by horizontal diffusion (light blue line) which is almost absent in H. It moves heat away from the warmpool towards higher latitudes and the equator. This happens, but to a lesser degree, south of the equator as well. The horizontal diffusion in L, which represents the mixing of the unresolved mesoscale eddy field, apparently overestimates the mixing of the eddies away from the equator. However, between 2^oS and 2^oN the Shapiro filter (Figure 5, light blue) performs surprisingly well and reproduces approximately 85% of the eddy heat flux convergence (Figure 4, dark blue). Thus, while in the ocean interior the eddies seem to move heat around adiabatically (Gill et al., 1973; Gent and McWilliams, 1990), they can lead to diabatic heating in the ML which suggests that there they can be represented by simple diffusion. This fact, that the eddies act differently in the interior and the surface is not captured well in current eddy parameterizations (Ferrari and McWilliams, 2004).

It should be noted that in L, unlike H, the heating of the ECT comes at the expense of the warmpool. In H, the area from 4^oS and 2^oN is heated with $2.4 \times 10^7 W/m$ whereas the area from 2^oN and 4^oN is only cooled with a rate of $0.4 \times 10^7 W/m$. This supports the dynamical analysis of JMB who show that the TIWs are caused by barotropic rather than baroclinic instability. Baroclinic instability implies an adiabatic flattening of isotherms in which water from the warmpool is moved on top of the ECT water. In H, only little warm pool heat is lost due to the TIWs (this also indicates that the breaking of TIW-crests is only of minor importance). Rather, the TIWs advect cold water poleward where it experiences a strong atmospheric heat flux and return it half a wave period later as warm water. A simple calculation can illustrate the power of this heat engine: the typical ML depth is 30 m, the average atmospheric heat flux is 100 W/m^2 and the TIW wave period is about 30 days. In the absence of other processes, the water parcel would return to the ECT 1 K warmer - which yields the 2 K/month heating rate of the TIWs in H (Figure 4). Of course, the gain would be same if the parcel did not move, but *only* if the entrainment cooling was switched off. Thus, the key to explain the strong heating of the TIWs is that they move the water away from the equatorial cooling, let it heat up by the atmosphere and then return it. At the equator the heat is then entrained into the thermocline by the strong vertical mixing. Thus, TIWs do not advect heat away from the tropical warmpool, rather they act, together with the strong vertical mixing at the equator, as a vertical heat pump that takes heat from the atmosphere and puts it into the thermocline. This result is not unique to the present model or the Atlantic TIWs. Revisiting earlier studies shows that this also happens in z-level models with SST restoring (JMB) or in the equatorial Pacific (Kessler et al., 1998).

We must emphasize that the above description of the mechanism by which the TIWs transport heat is extremely simplified. It is highlighted here because it represents a paradigm shift in the way to think about TIW heat fluxes - away

from simple mixing length arguments towards nonlocal effects of entrainment and atmospheric heat flux. Of course, the TIW heat flux convergence also has a component due to wave breaking (e.g.; Kessler et al., 1998), zonal (e.g.; Weingartner and Weisberg, 1991) and vertical (JMB) wave fluxes, none of which is necessarily negligible. However, a detailed discussion of these different contributions is beyond the scope of the present hypothesis and will be published in a separate study.

Another important result is that the entrainment cooling (green line) in L is *less* than in H (by approximately 20% when averaged between 2^oS and 2^oN). Thus, higher horizontal resolution leads to an increased downward diffusion of heat. The model's ML computes the entrainment from buoyancy forcing, wind-stirring and vertical shear instability. The wind stress is the same in both experiments and the buoyancy forcing is very similar (see later in the text) leading to a similar seasonal cycle in entrainment cooling (Figure 6). Thus, the difference must come from stronger shears below the ML. The entrainment cooling is largest near the equator because strong Ekman suction leads to a minimum in ML depth. There, the onset of the strong cooling in early spring coincides with a three fold increase of the equatorial wind stress from April to July. In contrast to L, the cooling in H continues to strengthen after June and is larger than in L until late fall when the winds start to weaken in response to the approaching ITCZ. The ML depth and stratification are only marginally different between H and L, therefore the larger entrainment in H must be due to to larger vertical shears in velocity which is significantly larger in H than in L (Figure 7).

The comparison of Q_{ent} in H and L (Figure 6) suggests that the shear only contributes from May to November, which is exactly the time in which the velocity difference between ML and EUC in H exceeds 0.8 m/s (Figure 7, for a review of EUC dynamics see Pedlosky, 1996). This large threshold is consistent with the findings of Chen et al. (1994) that adding shear instability to the Krauss-Turner mixing scheme of their *coarse* resolution model does not change the SST significantly. The empirical threshold of a velocity difference of 0.8 m/s between EUC and ML suggests a critical bulk Richardson number of approximately 0.7. This is close to 0.65, the threshold value that leads to instant vertical mixing in the successful mixing scheme of Price et al. (1986). Unlike the gradient Richardson number (Ri), which is based on shears between two adjacent layers, the bulk Richardson number is based on shears over a larger vertical extent, in this case the shear between surface and EUC core. The model employs a critical Ri of 0.25, which should have been sufficient to analyze the entrainment. However, we find that reevaluating Ri from the model output is not helpful in analysing the results, because the model fields are saved *after* the mixing has taken place. Furthermore, the shear mixing may involve successively all layers from the surface down to the EUC, making it difficult to use Ri criteria locally.

It is not obvious whether the increased shear that leads to the larger entrain-

ment in H is due to faster mean currents or due to TIWs, which are absent in L but of realistic strength in H (Jochum et al., 2004b). Distinguishing between these two effects is difficult because the TIWs are generated by barotropic instability of the Equatorial Undercurrent (JMB). Thus, the seasonal cycle of the EUC leads to a seasonal cycle of the TIW induced mixing which obstructs its quantification. An estimate of the relative importance of the TIW induced shear can be obtained as follows: The equatorial currents maintain their structure over the distance of one TIW wave length (800 - 1000 km), therefore averaging the velocity field from 26^oW to 18^oW will significantly reduce the impact of the TIWs on the shear but retain the shear of the mean currents (time-averaging over the average TIW period leads to similar results). Hence, we will compare

$$\langle((u_{surface} - u_{EUC})^2 + (v_{surface} - v_{EUC})^2)^{1/2}\rangle$$

with

$$((\langle u_{surface}\rangle - \langle u_{EUC}\rangle)^2 + (\langle v_{surface}\rangle - \langle v_{EUC}\rangle)^2)^{1/2}$$

where $\langle\rangle$ denotes an average from 26^oW to 18^oW. The first measure of shear retains the component due to the TIWs whereas the second one averages over one wavelength, thereby minimizing the impact of the TIWs on the shear. The difference between the 2 measures of vertical shear is rather small (Figure 7), suggesting that TIW induced shear makes only a small contribution to the vertical shear (this is true for the shear between any other two layers as well). Thus, the difference in entrainment between H and L is mostly due to an increased current strength. The SEC at the surface is directly driven by the wind and is not significantly different in H and L, but the EUC velocities are approximately 30% weaker in L compared to H, making the faster EUC the main reason for the stronger entrainment there.

A surprising result of the present comparison is that the atmospheric warming of the ECT is larger in H than L - by 15% when averaged from 2^oS to 2^oN - although the SST is larger in H than in L (Figures 3, 4 and 5). Since the incoming solar radiation is identical in both cases and the outgoing longwave radiation is increasing with SST, the difference must be due to differences in the sensible and latent heat fluxes. The total annual difference in heat flux is 14 W/m^2, 30% of which is contributed by sensible heat flux and 70% by latent heat flux (Figure 8). In standard heat flux parameterization schemes both sensible and latent heat loss would be larger in H because of the larger SST. In the present ABLM the advection of heat and moisture can change this simple local balance (Murtugudde et al., 1996). In the case of the ECT, warm and moist air is advected from south of the equator by the South-East Trades. Because the SST gradients are much

sharper in H than in L (Figures 3 and 9), the warming is larger in H. This effect is particularly strong in July when the Trades and the ECT are so strong that the sensible heat flux in H can *heat* the ML (Figure 8).

4 Summary and Discussion

Based on literature of tropical ocean modeling and TIWs we were led to the hypothesis that resolving TIWs in OGCMs will remove the cold bias of the ECT in coarse resolution OGCMs. This hypothesis was rejected with the analysis given in the present paper; however we gained new insights into details of the equatorial ML heat budget which are reported here. The most important result is that TIWs do *not* heat the ECT with heat from the warmpool. Instead they draw their heat from the atmosphere. In L, the diffusion that represents the TIWs heats the ECT by drawing heat from the warmpool, decreasing the SST there. With the ABLM we quantified this effect; spurious diffusion leads to approximately 1K cooler extra-equatorial tropics.

Secondly, better resolution leads to stronger vertical mixing and stronger cooling in the ECT which offsets the increased warming due to the TIWs. This is due to a stronger EUC and the associated larger vertical velocity shear which increases shear instability. This implies that in H, although the total oceanic heat flux convergence is similar to L, more heat is pumped into the equatorial thermocline, leading to a 20% weaker stratification in the upper 100 m (compared to L).

A third difference between H and L is found in the sensible and latent heat fluxes. The South-East Trades advect moist and warm air across the ECT which reduces the latent and sensible heat flux there. Although the ECT is warmer in H, this effect is larger there because of the sharper SST gradient. However, the meridional SST gradient is more realistic in L than in H (Figure 3), suggesting that the effect of atmospheric advection of heat and moisture is exaggerated in H. The caveat is that in reality the winds would respond to a changed SST. Therefore this particular result is a likely a numerical artifact, which emphasizes the importance of using a dynamic atmosphere in studies of the upper ocean.

Clearly, higher resolution does not remove or improve the cold bias of the ECT in this numerical model. Since the reason for this is the increased shear instability of the EUC whose effect is commonly parameterized, this particular result may differ from model to model. However, independent of the model is the finding that in coarse resolution models TIWs cannot be represented by lateral diffusion. Rather than moving heat laterally from the warm pool to the cold tongue, the TIWs, together with the increased shear instability of the EUC, move

heat vertically from the atmosphere into the thermocline. This requires a new parameterization which will be the focus of the authors future work.

The original hypothesis too explain the cold-tongue bias was rejected, therefore a crucial component of the ECT heat budget is still missing. It is not clear whether the missing component produces simply an offset or contributes to the seasonal cycle as well. Comparison of the seasonal cycles of SST in H, L and the observations shows that not only the mean SST is too cold in the model ECT, but also that the seasonal cycle of the SST is too weak. Moreover, the amplitude is independent on the resolution (Figure 10). The model produces not enough warming during fall and not enough cooling during spring. These differences could be removed by adding a correction of less than 20 W/m^2 during fall (about the uncertainty of the observed ocean-atmosphere heat flux) and removing it again during spring, but it is difficult to justify these corrections on physical grounds. Most certainly, the amplitude problem rules out a systematic error in the solar radiation data. Similarily, uniformly changing the drag coefficient that converts wind speed into wind stress, or the bouyancy and wind-stirring coefficients that determine the ML depth is unlikely to improve the solution over all. It may improve the SST during one season but only at the expense of a worse performance during other seasons. This was seen already for the annual mean SST by Murtugudde et al. (1996): changing the above parameters to improve the SST in the ECT worsens the SST elsewhere.

Of course there is a long list of physical processes that could improve the seasonal cycle but have been omitted in the present model configuration. For example, seasonal variations in high-frequency wind forcing or the diurnal cycle in the buoyancy forcing could be relevant. Since the thermodynamics of the ML is nonlinear these processe could make an important contribution to the heat budget. Hashizume et al. (2001) and Chelton et al. (2001) both observe strong coupling between the TIW induced SST anomalies and the local wind stress. These effects can possibly be parameterized and included into the ABLM to study whether this local coupling makes a net contribution to the ML heat budget. Another interesting process is discussed by Murtugudde et al. (2002) who find that the oceanic chlorophyll distribution leads to spatial variations in the attenuation depth of solar radiation. They show that, compared to constant attenuation depth, spatially variable attenuation depth can increase the mean SST in the ECT by more than 1K. Providing all these different processes with a sound physical representaion for a high resolution OGCM is not trivial and the authors expect their research in the near future to be devoted to this task.

Acknowledgements: The authors thank Gregory Foltz, Antonio J. Busalacchi and one anonymous reviewer for helpful suggestions. This research was funded with NOAA grant NA16GP1576 and NASA grant NAG5-7194 at MIT.

References

Blumenthal, M., Cane, M., 1989. Accounting for parameter uncertainites in model verification: An illustration with tropical SST. J.Phys.Oceanogr. 19, 815–830.

Cane, M., Dolan, S., Zebiak, S., 1986. Experimental forecasts of the 1982/83 El Nino. Nature 321, 827–832.

Chelton, D. B., Esbensen, S. K., Schlax, M. G., Thum, N., Freilich, M. H., Wentz, F. J., Gentemann, C. L., McPhaden, M., Schopf, P. S., 2001. Observations of coupling between surface wind stress and sea surface temperature in the eastern Tropical Pacific. J.Climate 14, 1479–1498.

Chen, D., Rothstein, L., Busalacchi, A., 1994. A hybrid vertical mixing scheme and its applications to tropical ocean models. J.Phys.Oceanogr. 24, 2156–2179.

Chiang, J., Kushnir, Y., Giannini, A., 2002. Deconstructing Atlantic ITCZ variability. J.Geophy.Res. 107, 10.1029.

Davey, M., coauthors, 2002. STOIC: A study of coupled model climatology and variability in tropical ocean regions. Climate Dynamics 18, DOI 10.1007/s00382–001–0188–6.

De Boyer Montegut, C., Fischer, A., Lazar, A., Iuducone, D., Madec, G., 2004. A global mixed layer depth based on individual profiles. J. Geophys. Res., submitted .

Ferrari, R., McWilliams, J. C., 2004. Parameterization of eddy fluxes at the ocean boundaries. Ocean Modelling, submitted .

Foltz, G., Carton, J., Chassignet, E., 2004. Tropical instability vortices in the Atlantic Ocean. J. Geophys. Res. 109, C03029.

Foltz, G., Grodsky, S., Carton, J., McPhaden, M., 2003. Seasonal mixed layer heat budget of the tropical Atlantic ocean. . J.Geophys.Res. 108, 10.1029.

Gent, P., Cane, M., 1989. A reduced gravity, primitive equation model of the upper equatorial ocean. J.Comput.Phys.. 81, 444–480.

Gent, P., McWilliams, J., 1990. Isopycnal mixing in ocean circulation models. J.Phys.Oceanogr. 20, 150–155.

Gill, A., Green, J., Simmons, A., 1973. Energy partition in the large-scale circulation and the production of mid-ocean eddies. Deep-Sea Res. 21, 499–527.

Hansen, D., Paul, C., 1984. Genesis and effects of long waves in the equatorial Pacific. J.Geophys.Res. 89, 10431–10440.

Hashizume, H., Xie, S., Liu, T., Takeuchi, K., 2001. Local and remote atmospheric response due to tropical instability waves: A global view from space. J.Geophys.Res. 106, 10173–10185.

Hellerman, S., Rosenstein, M., 1983. Normal monthly wind stress over the world ocean with error estimates. J.Phys.Oceanogr. 13, 1093–1104.

Inui, T., Lazar, A., Malanotte-Rizzoli, P., Busalacchi, A., 2001. Wind stress effects on the Atlantic tropical-subtropical circulation. J.Phys.Oceanogr. 32, 2257–2276.

Jochum, M., Malanotte-Rizzoli, P., Busalacchi, A., 2004a. Tropical Instability Waves in the Atlantic Ocean. Ocean Modelling 7, 145–163.

Jochum, M., Murtugudde, R., Malanotte-Rizzoli, P., Busalacchi, A., 2004b. Internal variability in the Atlantic Ocean. in: Ocean-Atmosphere Interaction and Climate Variability, Geophys. Monogr. Ser., edited by Wang, Xie and Carton 147, 181–187.

Kessler, W. S., Rothstein, L. M., Chen, D., 1998. The annual cycle of SST in the eastern tropical Pacific as diagnosed in an OGCM. J. Clim. 11, 777–799.

Kraus, E., Turner, J., 1967. A one-dimensional model of the seasonal thermocline. Part II. Tellus 19, 98–105.

Levitus, S., 1994. Climatological Atlas of the World Ocean. NOAA Prof. Paper 13 .

Li, Z., Leighton, H., 1993. Global climatologies of the solar radiation budgets form 5 years of ERBE data. J. Geophys. Res. 98, 4919–4930.

Lorenz, E., 1971. An N-cycle time-differencing scheme for stepwise numerical integration. Mon.Wea.Rev 99, 644–648.

Murtugudde, R., Beauchamp, J., McClain, C., Lewis, M., Busalacchi, A., 2002. Effects of penetrative radiation on the upper tropical ocean circulation. J.Climate 15, 470–486.

Murtugudde, R., Seager, R., Busalacchi, A., 1996. Simulation of the tropical oceans with and ocean GCM coupled to an atmospheric mixed layer model. J.Climate 9, 1796–1815.

Nurser, A., Zhang, J., 2000. Eddy-induced mixed layer shallowing and mixed layer/thermocline exchange. J.Geophys.Res. 105, 21851–21868.

Oschlies, A., 2002. Improved representation of upper ocean dynamics and mixed layer depths in models of the North Atlantic ocean. J.Phys.Oceanogr. 32, 2277–2298.

Pacanowski, R., Philander, S., 1981. Paramterization of vertical mixing in numerical models of the oceans. J.Phys.Oceanogr. 11, 1443–1451.

Pedlosky, J., 1996. Ocean Circulation Theory. Springer.

Price, J., Weller, R., Pinkel, R., 1986. Diurnal cycle: Observations and models of the upper ocean response to diurnal heating, cooling and wind mixing. J.Geophys.Res. 91, 8411–8427.

Reynolds, R., Smith, T., 1994. Improved global SST analyses using optimal interpolation. J.Climate 7, 929–948.

Rossow, W. B., Schiffer, R. A., 1991. ISCCP Cloud data products. Bul. Amer. Meteor. Soc. 72, 2–20.

Seager, R., Blumenthal, M., Kushnir, Y., 1995. An advective atmospheric mixed layer model for ocean modeling purposes: global simulation of atmospheric heatfluxes. J.Climate 8, 1951–1964.

Stevenson, J., Niiler, P., 1983. Upper ocean heat budget during the Hawaii-to-Tahiti shuttle experiment. J.Phys.Oceanogr. 13, 1894–1907.

Stockdale, T. and coauthors, 1993. Intercomparison of tropical ocean GCMs. World circulation programme research, Memo WCRP-79, 67pp.

Weisberg, R., Weingartner, T., 1988. Instability Waves in the equatorial Atlantic Ocean. J.Phys.Oceanogr. 18, 1641–1657.

Weisberg, R., Weingartner, T., 1991. A description of the annual cycle in SST and upper ocean heat in the equatorial Atlantic. J.Phys.Oceanogr. 21, 83–96.

Xie, P. P., Arkin, P. A., 1998. Global monthly precipitation estimates from satellite-observed outgoing longwave radiation. J. Clim. 11, 137–164.

Zebiak, S., 1993. Air-sea interaction in the tropical Atlantic. J.Climate 6, 1567–1586.

Figure 1: Annual mean of the SST, superimposed is the variance of the meridional velocity in the mixed layer (contour lines: $100cm^2/s^2$, the maximum is $1800cm^2/s^2$). The seasonal cylce has been removed from the velocity before computing the variance.

Figure 2: Mixed Layer depth averaged between 25^oW and 20^oW for the observations (from de Boyer Montegut et al., 2004, solid line), for H (dashed line) and L (dotted line). A longitudinal section of the annual mean is shown in the upper figure and the seasonal cycle at the equator is shown in the lower figure. Note that in the model the mixed layer depth is a prognostic variable whereas in the observations it cannot be defined based on first principles. Especially in areas of weak stratification the mixed layer depth can vary significantly for slightly different definitions.

Figure 3: Annual mean SST averaged between 25^oW and 20^oW for Reynolds and Smith (1994, black line: mean; blue lines: ± 1 standard deviation), H (red line) and L (green line). The close similarity in SST between the observations and H north of 2^oN is not the result of any parameter tuning but should not be taken as an indication of a perfect model either. The important point is that SST in H is increased *and* improved.

Figure 4: Annual mean heat budget for H averaged between 25^oW and 20^oW. Black: net surface heat flux; Red line: mean and seasonal advection of heat; Dark Blue: eddy heat fluxes; Light Blue: horizontal diffusion; Green: entrainment and vertical diffusion. Units are Kelvin/month.

Figure 5: As previous Figure for L. Eddy heat fluxes are negligible.

Figure 6: The annual cycle of entrainment on the equator, averaged between 25^oW and 20^oW. Solid line: L. Broken Line: H.

Figure 7: The seasonal cycle of the velocity difference on the equator between South Equatorial Undercurrent (SEC) and Equatorial Undercurrent (EUC) for L (solid line), H (dashed line) and H with TIWs filtered out (dotted line).

Figure 8: The seasonal cycle of the latent (top) and sensible heat flux (bottom) at the equator between 25^oW and 20^oW for H (dashed line) L (solid line). Note the difference in scale.

Figure 9: The July SST in the central tropics for H (colored) and L (contour lines every 0.5 K). Overlaid is the July wind stress. Note how the South-East

Trades blow from warm water to the cold water in the ECT in both experiments but cross more isotherms in H.

Figure 10: Seasonal cycle of SST averaged between 25^oW and 20^oW and between 1^oS and the equator for Reynolds and Smith (1994, solid line), H (dashed line) and L (dotted line).

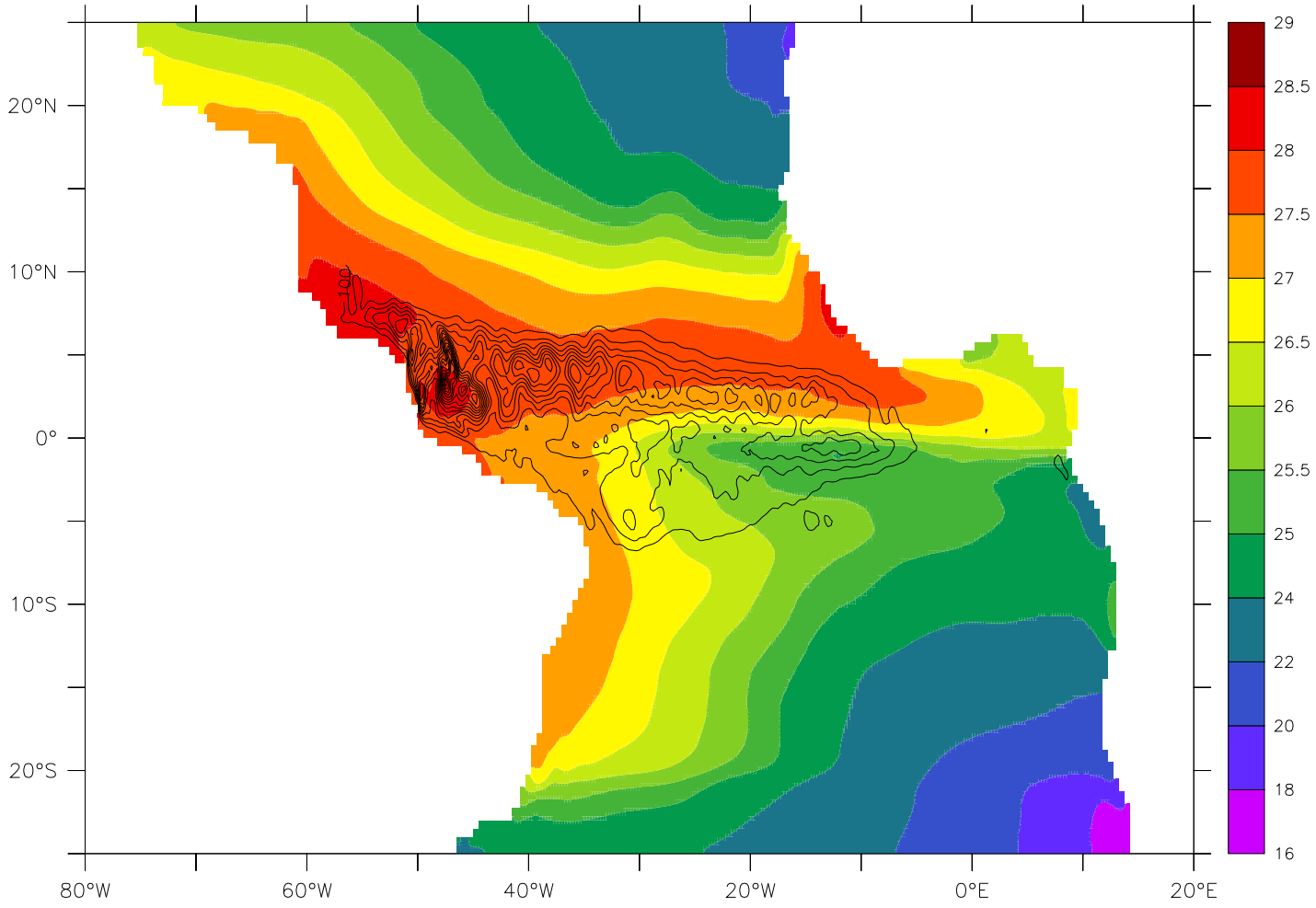
20°N
10°N
0°
10°S
20°S
80°W
60°W
40°W
20°W
0°E
20°E
100
29
28.5
28
27.5
27
26.5
26
25.5
25
24
22
20
18
16

Figure 1:

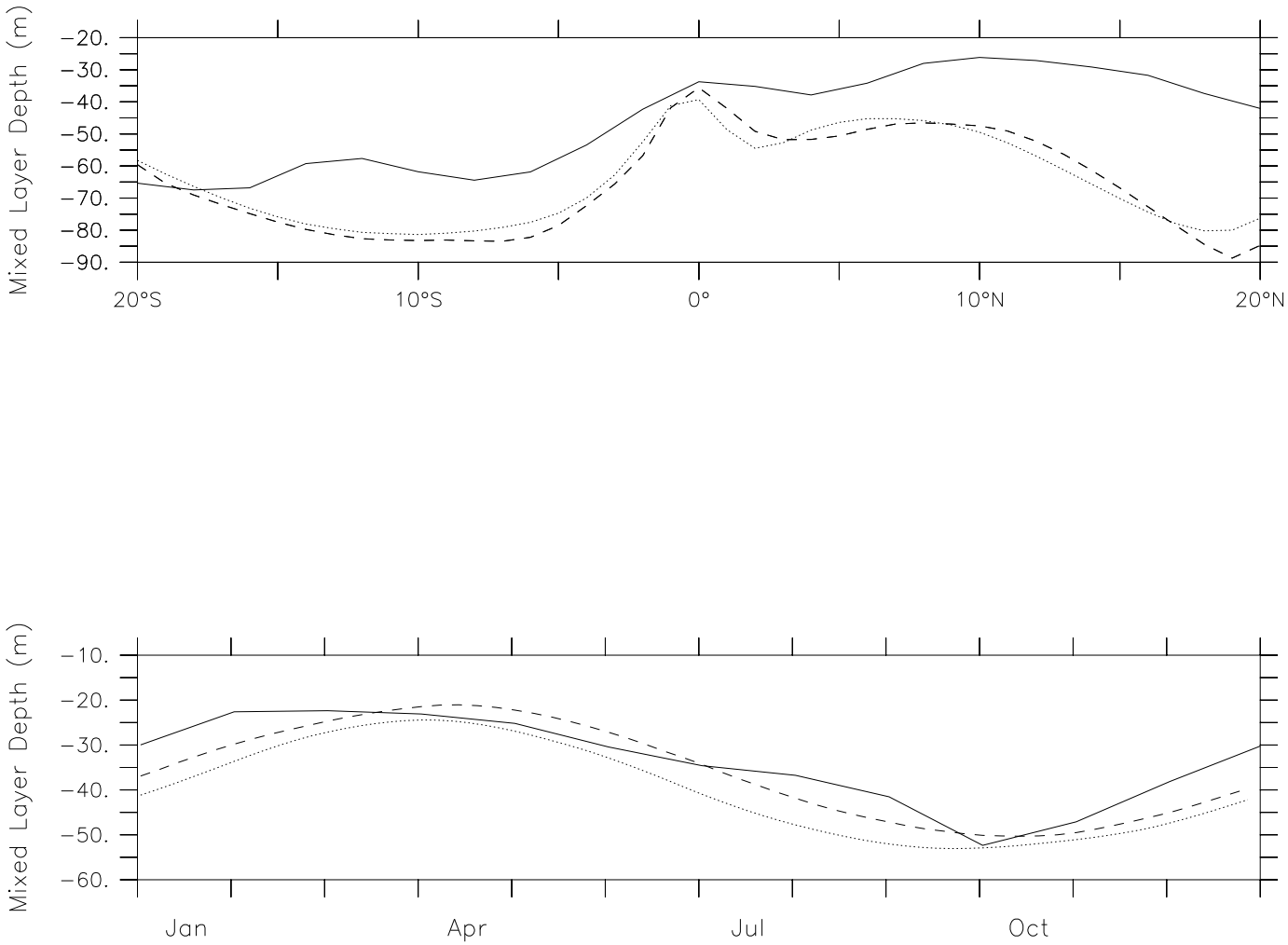
Mixed Layer Depth (m)
−20.
−30.
−40.
−50.
−60.
−70.
−80.
−90.
20°S
10°S
0°
10°N
20°N
Mixed Layer Depth (m)
−10.
−20.
−30.
−40.
−50.
−60.
Jan
Apr
Jul
Oct

Figure 2:

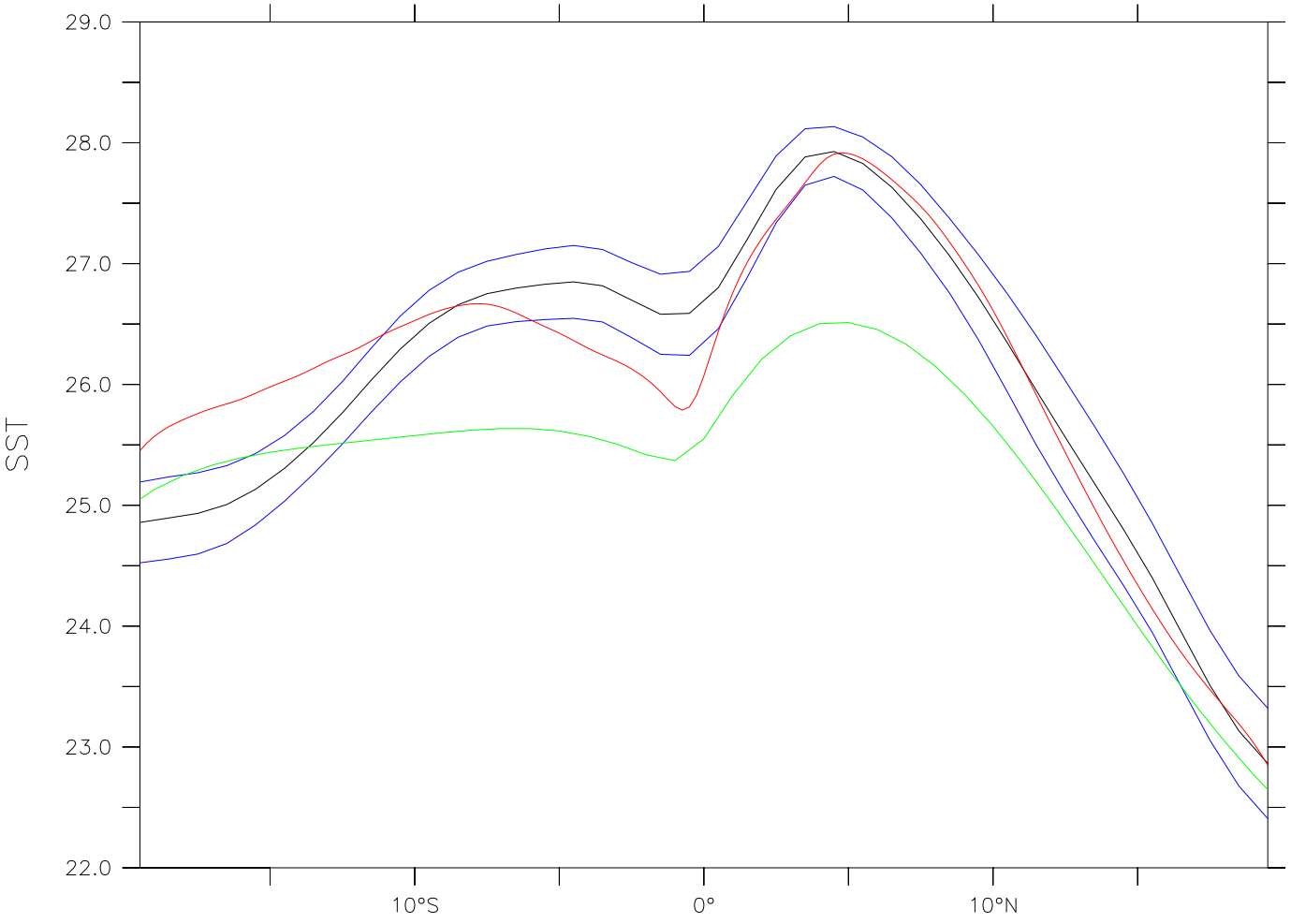

Figure 3:

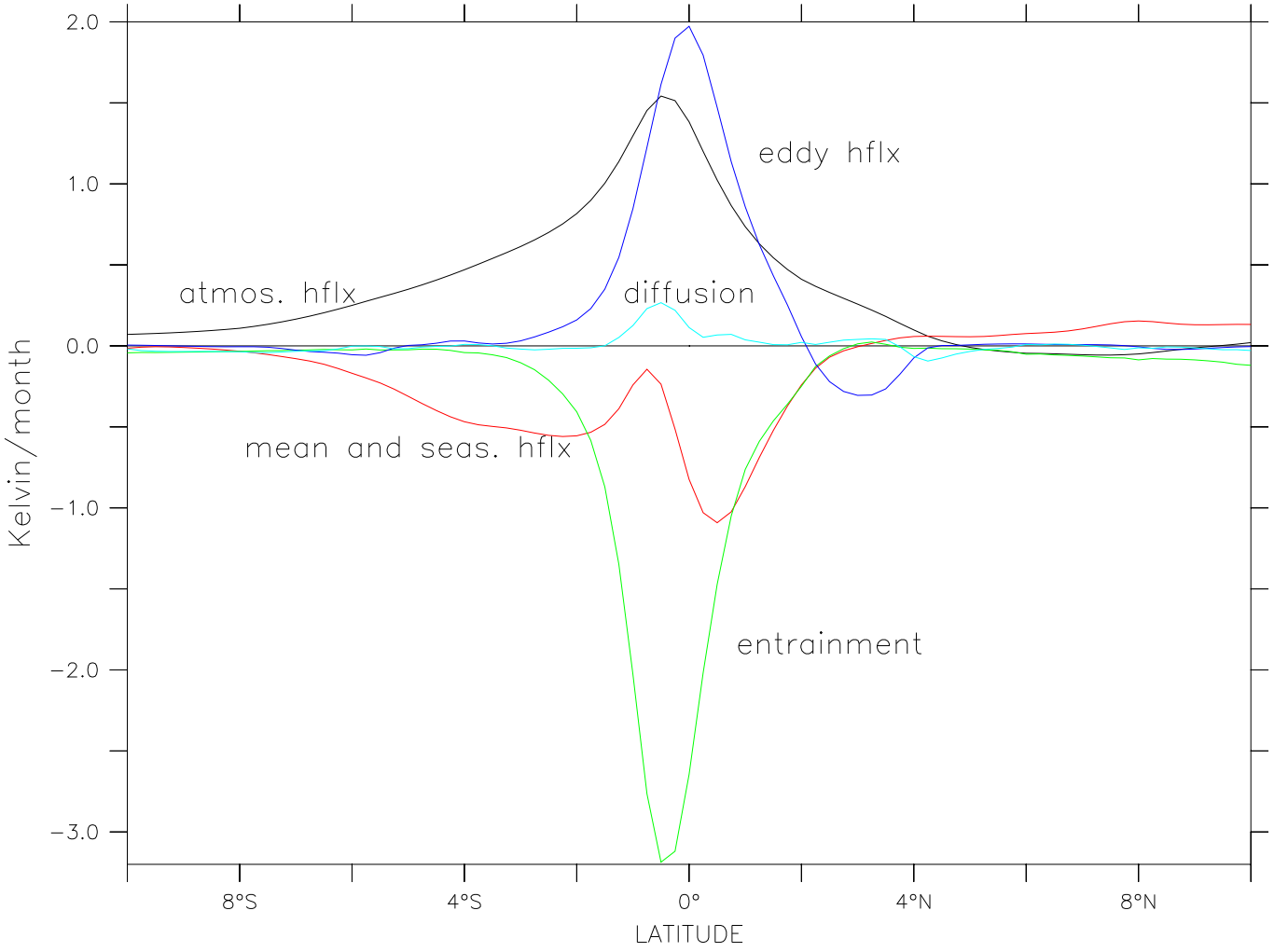
2.0
1.0
0.0
−1.0
−2.0
−3.0
Kelvin/month
eddy hflx
atmos. hflx
diffusion
mean and seas. hflx
entrainment
8°S
4°S
0°
4°N
8°N
LATITUDE

Figure 4:

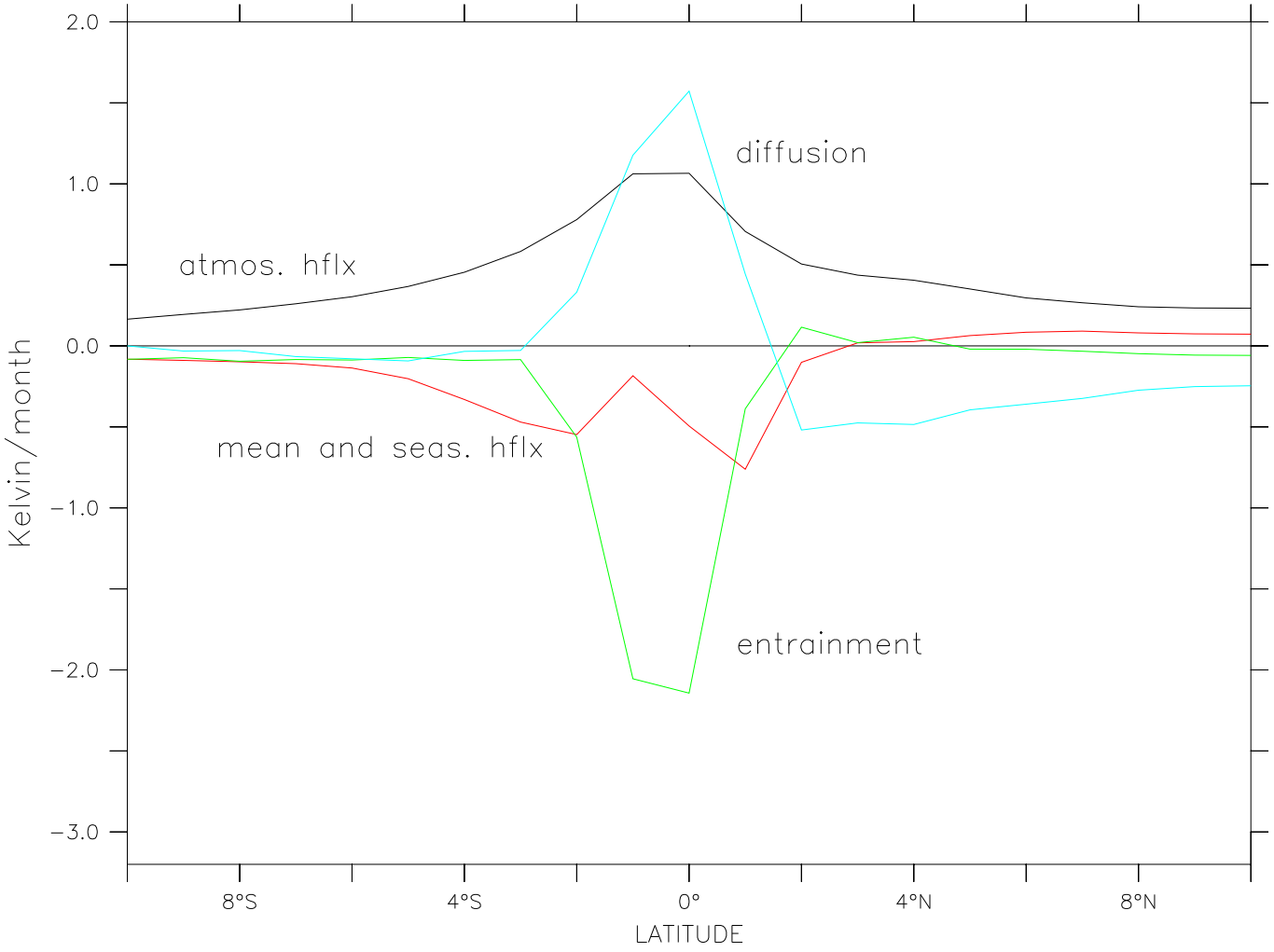
2.0
1.0
0.0
−1.0
−2.0
−3.0
Kelvin/month
diffusion
atmos. hflx
mean and seas. hflx
entrainment
8°S
4°S
0°
4°N
8°N
LATITUDE

Figure 5:

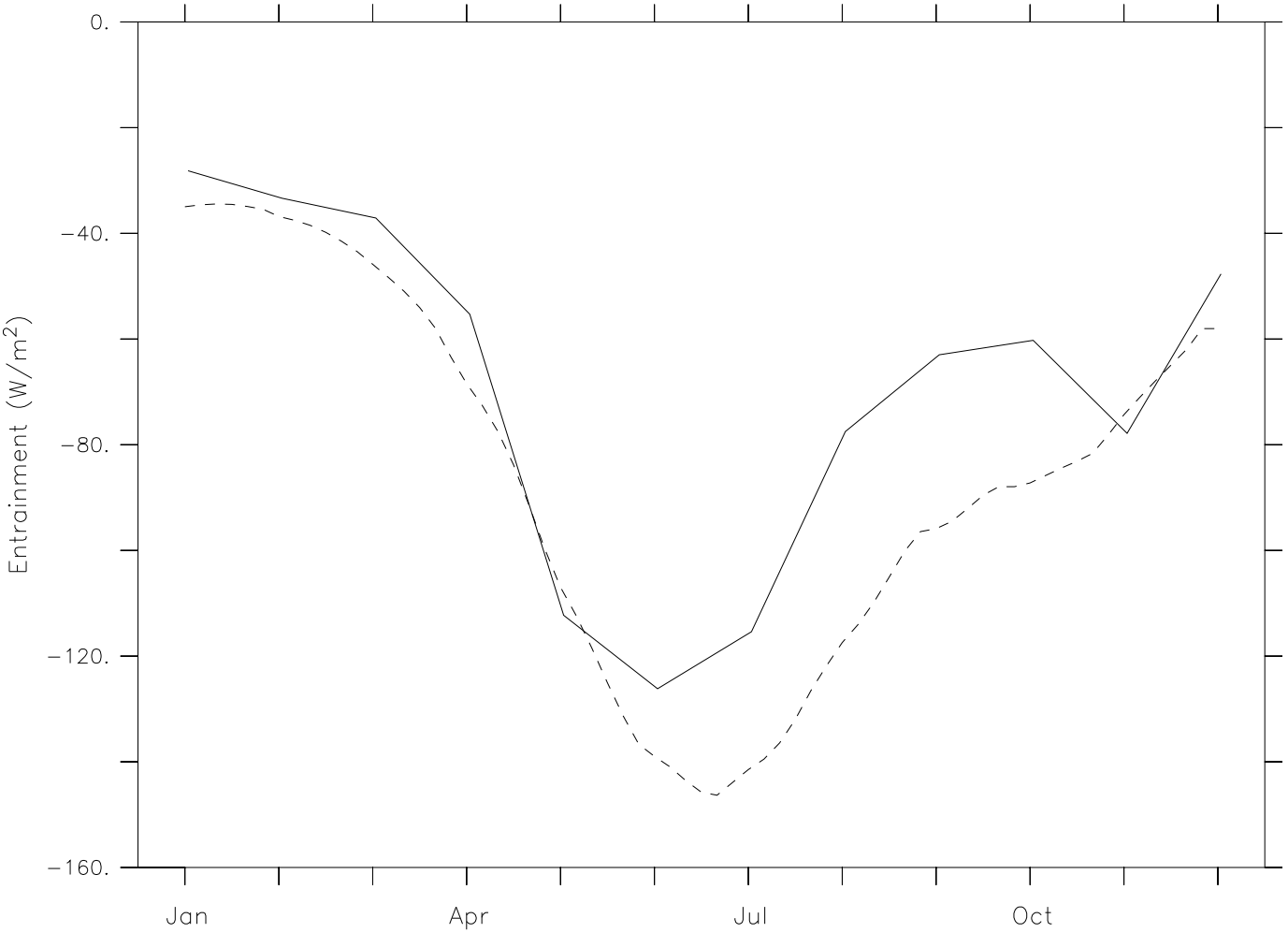

Figure 6:

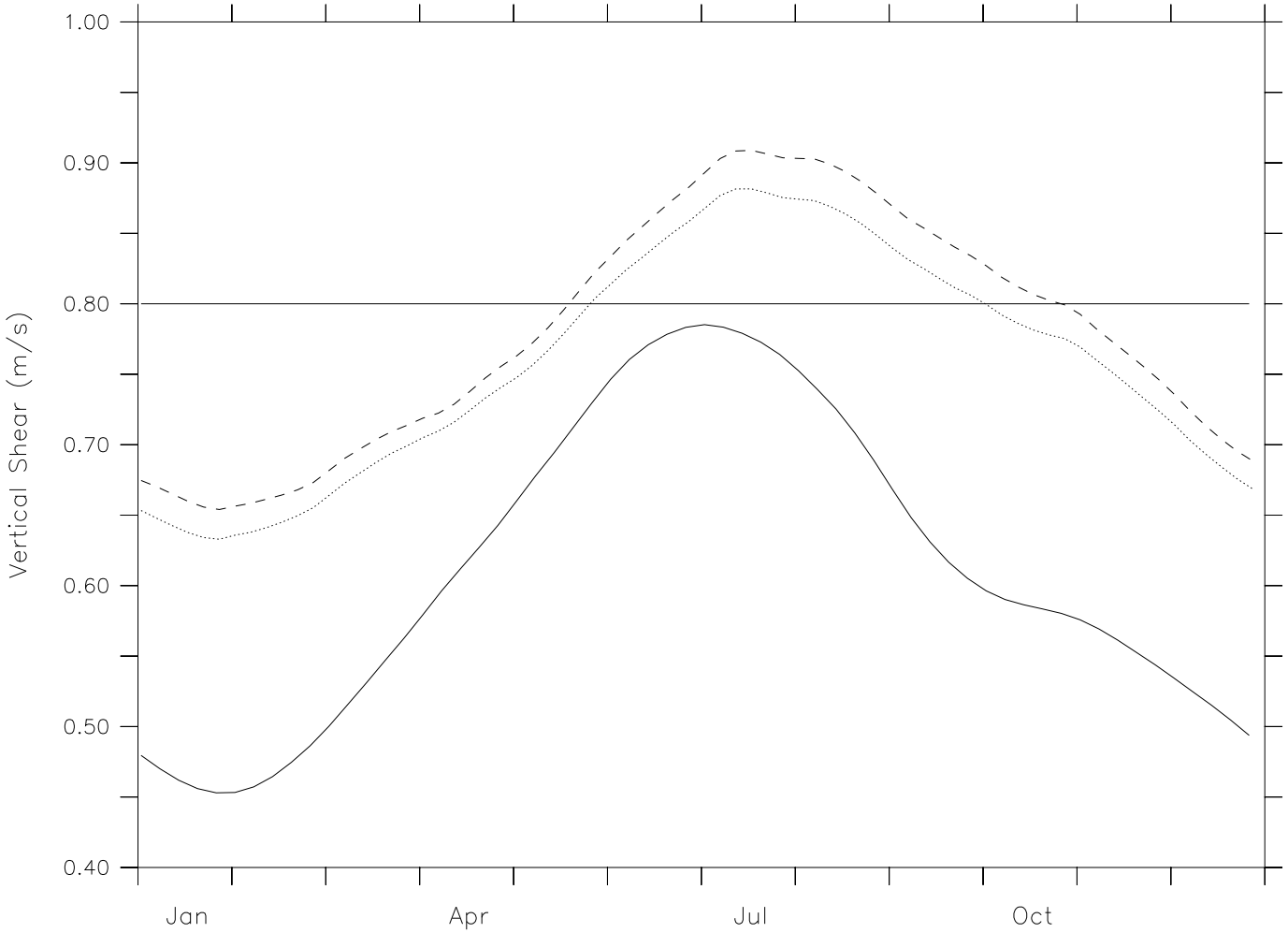

Figure 7:

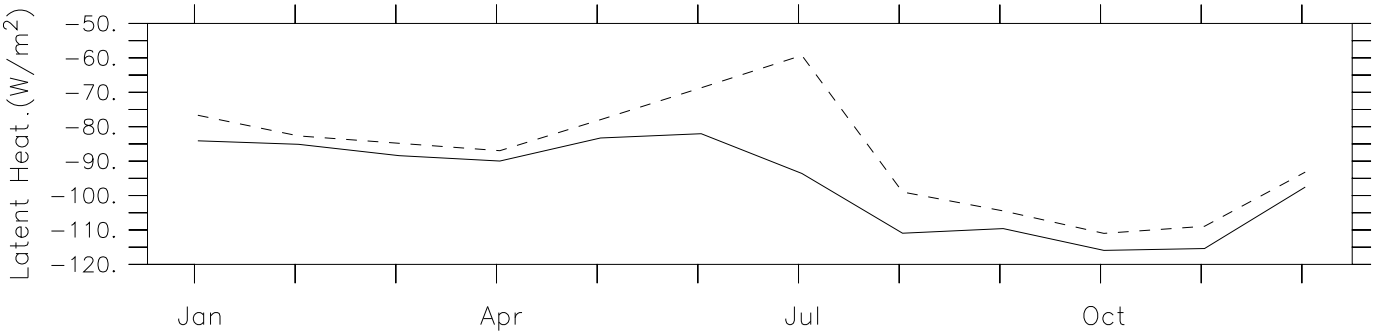
Latent Heat (W/m2)
−50.
−60.
−70.
−80.
−90.
−100.
−110.
−120.
Jan
Apr
Jul
Oct

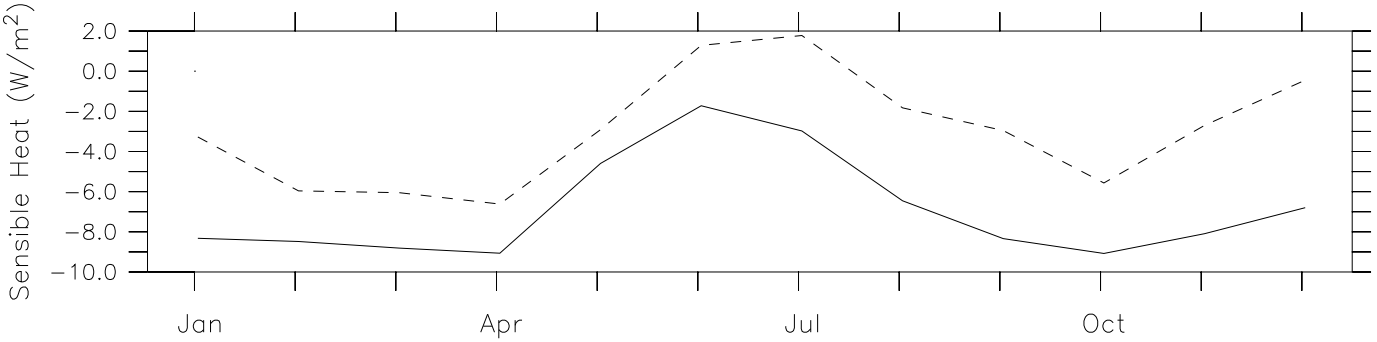
Sensible Heat (W/m2)
2.0
0.0
−2.0
−4.0
−6.0
−8.0
−10.0
Jan
Apr
Jul
Oct

Figure 8:

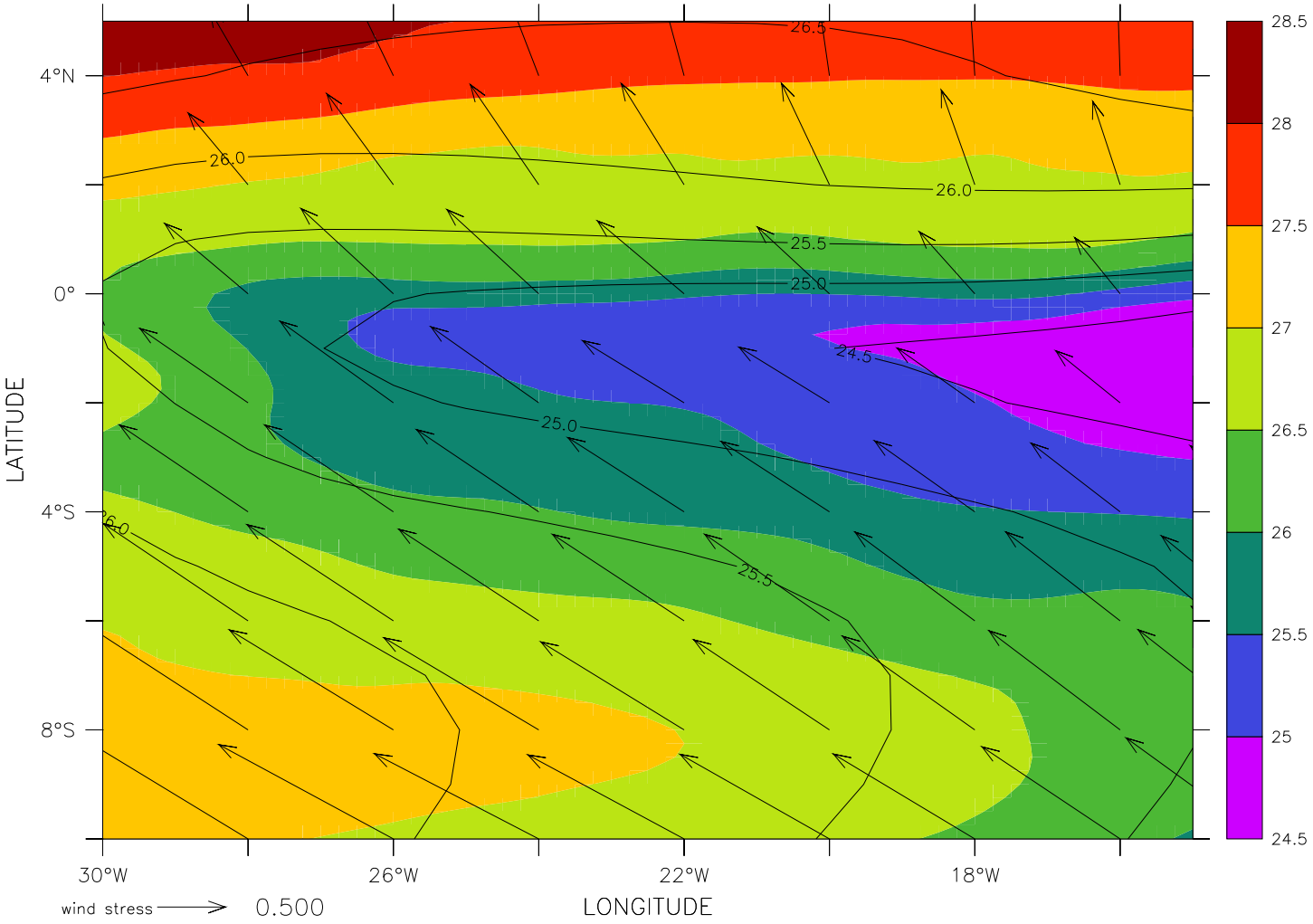
4°N
0°
4°S
8°S
LATITUDE
30°W
26°W
22°W
18°W
LONGITUDE
wind stress
0.500
26.5
26.0
25.5
25.0
24.5
28.5
28
27.5
27
26.5
26
25.5
25
24.5

Figure 9:

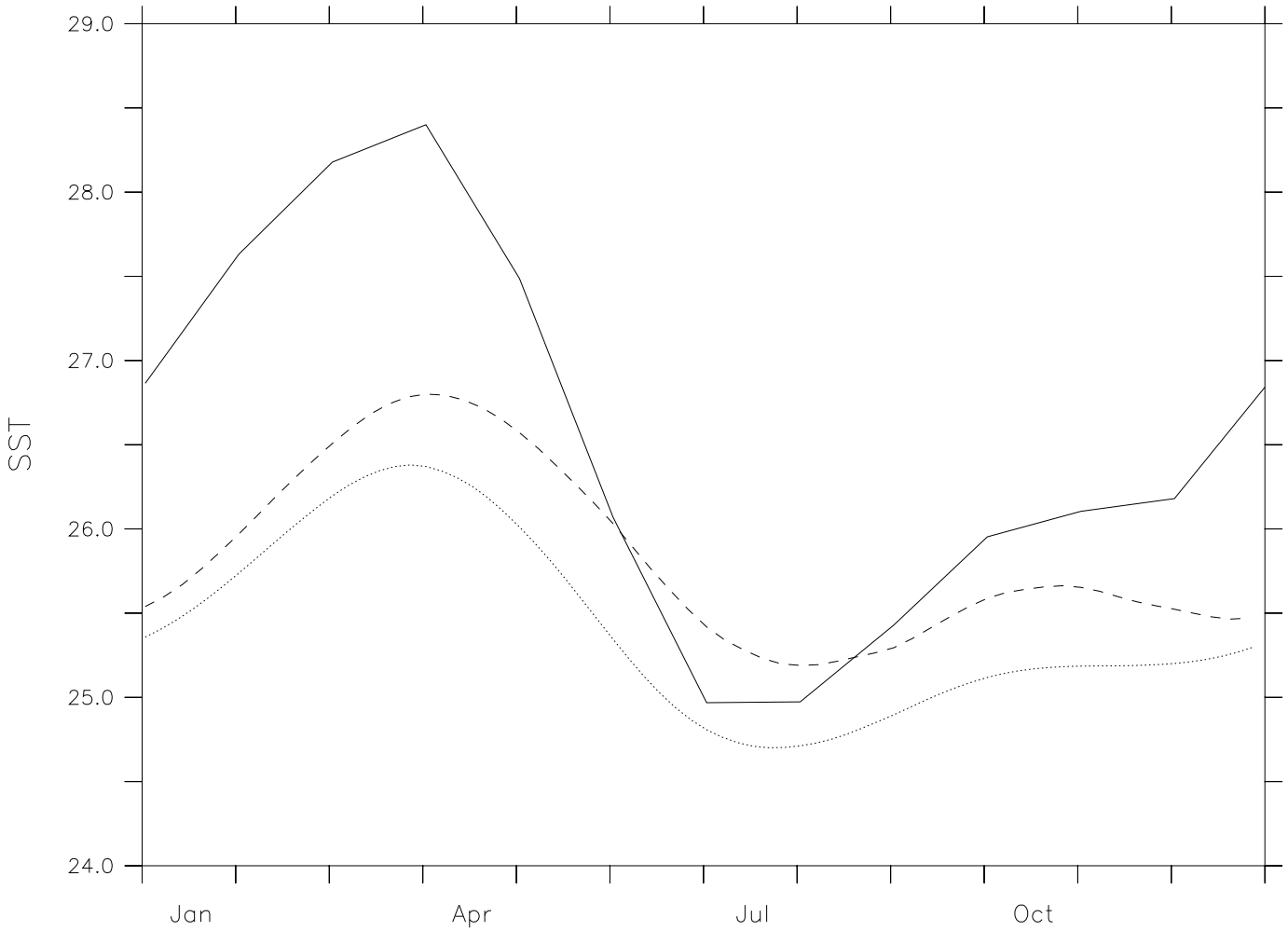

Figure 10: